Rapid Communications in Mass Spectrometry

Oxygen isotope analysis for silicate minerals using a high temperature conversion/elemental analyzer-isotope ratio mass spectrometer

Ryosuke Kikuchi*[1], Tobimaru Ishiwata[2], Ichiro Tayasu[3]

[1] Faculty of Engineering, Hokkaido University, Sapporo 060-8628, Hokkaido, Japan, [2] Graduate School of Engineering, Hokkaido University, Sapporo 060-8628, Hokkaido, Japan, [3] Research Institute of Humanity and Nature, Kita-ku, Kyoto, 603-8047 Japan.

*Corresponding author

Tel: +81-11-706-6320 (Ext: 6320)

E-mail address: rkikuchi@eng.hokudai.ac.jp

Keywords: thermal conversion, IRMS, silicate, oxygen isotope

Short title: O isotopes analysis for silicate using TC/EA-IRMS

ABSTRACT

RATIONALE: Oxygen isotope composition of silicates is an important indicator of the formation environment and/or subsequent geochemical processes of minerals. Compared to carbonate minerals and organic matter, silicate is a less common target for oxygen isotope measurements because of the need for specialized fluorination instruments to break strong Si-O bonds.

METHODS: We introduce a simple method using a high temperature conversion elemental analyzer-isotope ratio mass spectrometer (TC/EA-IRMS), which does not require specialized instrumentation. Silicate powder with various fluorine compounds and ratios of fluorine/oxygen were decomposed at 1450°C, and then, mass spectral characteristics, oxygen yields, and $\delta^{18}O$ values were compared.

RESULTS: NaF and KF were the most reactive fluorine sources, followed by polytetrafluoroethylene, LiF, CaF_2, BaF_2, and AlF_3, with decreasing reactivity. The F/O ratio affected the tailing of the CO peaks in the mass spectrum. Higher F/O ratios show a more rapid regression to background, resulting in higher reproducibility of oxygen yield and $\delta^{18}O$. In addition to simply adding fluorides to the sample, homogenization treatment also improved the reactivity. Activated carbon catalyzed by nickel is a better carbon source than graphite in terms of reactivity. The quartz and smectite with NaF added at an F/O ratio of 6 provided 90.0–99.3% of oxygen yields, $\delta^{18}O$ values that deviated less than 1.42‰ from literature values, and 0.18–0.30 ‰ of precision.

CONCLUSIONS: Although further investigation is required to verify its accuracy, the potential of the TC/EA-IRMS method for silicates is demonstrated. Because the hydrogen isotope composition can also be examined using the same instrument, it is expected that this method can be applied to a wider range of earth materials, including hydrous silicates such as clay minerals.

1. Introduction

Oxygen is the most ubiquitous element in Earth's crust. It exists in various gases (e.g., atmospheric O_2 and water vapor), liquids (e.g., water, oxygen-containing ions, and dissolved organic matter), and solid forms (e.g., organic matter and minerals). Oxygen is involved in most life processes and plays key roles in the biogeochemical cycling of other elements such as carbon, nitrogen and sulfur. The oxygen isotope composition as the per mil (‰) difference of the sample form the standard was defined using delta(δ) notation [1]:

$$\delta^{18}O = \frac{R_{sample}}{R_{standard}} - 1$$

where R is the ratio of the heavy isotope (^{18}O) to the light isotope (^{16}O) of the sample material relative to the isotope ratio of an international standard, Vienna Standard Mean Ocean Water (VSMOW).

Isotopic fractionation of oxygen occurs near the Earth's surface due to dynamic interactions between lithosphere, hydrosphere and atmosphere [2]. Therefore, oxygen isotopes are important tracers in all geologic processes, from igneous petrogenesis [3] to formation of ore deposit [4] and sedimentation [5, 6], to reveal the conditions (e.g., temperature) and the reservoirs involved in the reactions. Among the oxygen-bearing terrestrial materials, silicate minerals consist of 92% of the earth's crust [7] and thus, oxygen isotope in silicates have been intensively investigated for many years. However, compared to carbonate minerals and organic matters, oxygen isotope analysis for silicates faces greater technological challenges in extracting oxygen from silicates, in which strong covalent bonds exist between Si-O.

Several methods have been developed to extract oxygen from silicates. These include the traditional Ni-bomb fluorination using BrF_5 [8] and CO_2 laser fluorination under a fluorine gas atmosphere such as BrF_5 or ClF_3 [9]. The latter may involves mixing the sample with fluoride compounds such as LiF [10] or BaF_2 [11]. The addition of fluoride is expected to prevent the fine-grained samples from scattering during laser heating and/or maintain a high heating rate [10]. Current methodologies for fluorination depend on hazardous fluorine gases and specialized vacuum lines or laser instrument to break the covalent Si–O–Si bonds and transfer extracted oxygen to isotope ratio mass spectrometer (IRMS). These requirements may limit further expansion of oxygen isotope studies of silicate minerals.

The alternative methodology involving a thermal decomposition using a high temperature conversion elemental analyzer (TC/EA) has been proposed to use more widespread equipment [12, 13]. This TC/EA-IRMS method is expected to be a simple and safe method that does not use hazardous gases such as BrF_5, requires no specialized external apparatus, and requires less time for sample fluorination than conventional methods. However, despite their potential, there are not yet many applications for silicate minerals, and verification of pyrolysis methods is required. The most critical drawback of TC/EA-IRMS method is the low oxygen yield. If simply combusted, most of the oxygen will not be released. For example, Yin & Chen (2014) combusted SiO_2 at 1450°C and recovered only 2.0% [14]. Similarly,

Kornexl et al. (1999) obtained yields of only <10 % for silicate after combustion at 1400°C [15]. However, this low oxygen yield problem could be significantly improved by the addition of fluoride compound [12, 13]. Gehre & Strauch (2003) enhanced oxygen yields of silicates from <5% to >80% by adding KF or polytetrafluoroethylene (PTFE). Menicucci et al. (2013) obtained oxygen yields of 65 - 95% and 95-113% from quartz and biogenic silica with the addition of PTFE. The challenge of these methods of improving oxygen yields by additives is that oxygen yields vary even for the same sample, and the yields may deteriorate depending on the amount and particle size of the sample. Therefore, the optimization of additive recipes and adding procedure is required. Recently, a high temperature conversion-methanation-fluorination method for high-precision triple oxygen isotope analysis was also proposed that decomposes various earth materials, including silicates [16]. They enabled precise oxygen isotope measurements using dual-inlet IRMS combined with a stand-alone furnace for CO_2 methanation and H_2O fluorination, although some drawbacks also possess; incomplete oxygen recovery (~80%) from quartz, the highly complicated machine configuration and the large amount of sample (probably several mg).

A dual-inlet system was used to enable highly precise analysis through multiple gas generation/purification traps. By repeating the measurements for both purified sample gases and references, dual-inlet systems generally offer higher precision than continuous-flow IRMS; nevertheless, they necessitate larger sample volumes and longer pretreatment durations. For the high-throughput measurement of a large number of samples required in geoscience, it is necessary to establish the measurement method using a continuous-flow system and a simpler instrument configuration.

In this study, pyrolysis and oxygen isotope ratio measurements were performed using a TC/EA-IRMS in a continuous-flow system with a simple instrument configuration. Silicate minerals were mixed with fluorides using various recipes and thermally decomposed to produce CO gas. Their reactivity, oxygen yields, and $\delta^{18}O$ values obtained were compared. In addition to quartz, which is a typical silicate mineral, we also investigated its applicability to clay minerals, which are hydrous silicate minerals that cover the majority of the Earth's surface, to explore the potential for the continuous measurement of oxygen and hydrogen isotopes using the same instrument.

2. Experimental

2.1. Materials

Non-silicate samples, calcite (NBS18) and benzoic acid (IAEA-601, and -602), were used as calibration standards[17, 18]. NBS28 and SWy-1, for which $\delta^{18}O$ values have already been reported, were used as representative silicate mineral samples [11, 19]. NBS28 is quartz, which is a SiO_2 standard distributed by the IAEA. The Wyoming Na-montmorillonite SWy-1 is distributed in the source clay repository of the US Clay Mineral Society. SWy-1 has been widely used in several experiments as a

115 standard clay mineral. It consists of 90–95% montmorillonite and 5–10% quartz. All samples and
116 calibration standards were summarized in Table S1.
117 In some experiments (described in the next section) for checking only reactivity rather than $\delta^{18}O$
118 values, quartz powder with a particle size of 4 μm (99.9% purity, Kojundo Chemical Laboratory, Co.,
119 Ltd.) was also used instead of NBS28 to avoid consuming NBS28. This quartz sample will be referred
120 as the Qz sample from now on. Furthermore, samples of clay from locations other than SWy-1 were
121 employed. From the Tsukinuno bentonite mine in Yamagata Prefecture , Japan, three montmorillonite
122 samples were acquired [20]. They were chosen for this study because of their high montmorillonite
123 content and as an example of natural ores obtained from clay deposits.
124 In this study, fluorine and carbon compounds were added to the sample to enhance the CO gas
125 production during thermal decomposition. First, following previous studies [12, 13], PTFE was used as
126 the fluorine source. The following inorganic fluorides were also tested: KF, NaF, LiF, CaF_2, AlF_3
127 (FUJIFILM Wako Pure Chemical Corporation, 99%, 99%, 98.0%, 99.9%, 31.0–34.0 (as Al) % purity,
128 respectively), and BaF_2 (Kojundo Chemical Laboratory Co., Ltd., 99% purity). Graphite powder (5–
129 11 μm of particle size, AS ONE Corporation) was used as a carbon source. Granular nickelized carbon
130 (10 wt% Ni, Elemental Microanalysis Co., Ltd.) was also tested instead of graphite to enhance the
131 reaction. This carbon has been nickelized and is henceforth referred to as Ni/C. Ni/C is activated
132 carbon doped with metallic Ni nanoparticles; the doped Ni's catalytic function is thought to speed up
133 the pace at which gas is produced as organic matter breaks down [21].
134
135 2.2. Methods
136 2.2.1. Pre-treatment for clay samples
137 Pre-treatment for montmorillonite samples were performed by the following method: To remove
138 impurities such as quartz and feldspar, the clay fraction was extracted from the bentonite ores (TKN-
139 01, -29, and -31). The samples were dispersed in deionized water and placed in an ultrasonic bath to
140 aid in disintegration. After this, the samples were separated into the < 2 μm size fraction by
141 centrifugation based on Stoke's Law. Finally, the clay fractions were freeze-dried. The appropriate size
142 fraction was determined using powder X-ray diffraction, and no impurities were observed in any
143 fraction.
144 In order to obtain representative $\delta^{18}O$ values for clay minerals, removing adsorbed water molecules
145 is necessary. The majority of the adsorbed water linked to smectite is bound to the interlayer at ambient
146 temperature and humidity levels [22]. In this study, montmorillonite samples were ion-exchanged with
147 K^+, which has a low hydration enthalpy. The smectite saturated with K^+ was the least hygroscopic
148 compared to other exchangeable cations (Ca^{2+}, Na^+) and provided a more accurate H isotope ratio in
149 the structure [23]. In this study, K^+ saturation for the montmorillonite samples was achieved by dispersion
150 in a 2M KCl solution, shaking for 15 min, and solid-liquid separation by centrifugation. This procedure

was repeated three times to produce homoionic K^+-saturated forms of each sample. After saturation, the samples were dispersed in deionized water and shaken for 15 min to remove excess salt before solid-liquid separation. This procedure was repeated three times. The samples were then freeze-dried and gently ground into a fine powder using an agate mortar and pestle.

2.2.2. TC/EA configuration

The TC/EA-IRMS used in this study was in the standard configuration, except for a gas trap between the reactor and GC column (Fig. 1). The samples were inserted into a zero-blank autosampler (Costech), which contained a maximum of 99 samples (Fig. 1(a)). The autosampler was continually purged with He gas to remove atmospheric gases such as N_2, O_2, and H_2O. Thermal decomposition was performed after the samples fell into the TC/EA (Thermo Fischer Scientific) system. The central part of the TC/EA is a high-temperature reactor composed of an outer ceramic tube and an inner glassy carbon tube (Fig. 1(b)). The glassy carbon tube was filled with a layer of silver wool at the bottom and a layer of glassy carbon granule (several millimeters in size). The reaction residue was collected using a graphite crucible that was held up by glassy carbon granules. The crucible was positioned in the hottest zone of the reactor and was set at 1450˚C in this study.

The thermal decomposition of quartz (SiO_2) using this method is represented by the following reaction:

$$SiO_2 + 4NaF + 2{*}C \rightarrow 2{*}CO + SiF_4 + 4Na$$

Here, *C represents carbon derived from graphite or Ni/C powder. CO and fluoride gases were generated. Although the chemical species of the fluoride gases produced here have not been identified, it is assumed that they are mainly SiF_4. In the case of SiO_2 decomposition with PTFE, at least, the following two reactions are considered to be taking place simultaneously:

(1) $C_2F_4 \rightarrow CF_4\,(gas) + C_{excess}$

(2) $CF_4\,(gas) + SiO_2 + C_{excess} \rightarrow 2CO + SiF_4 + C_{excess}$

CF_4 gas is produced by PTFE decomposition (reaction 1), which is converted into more stable SiF_4 in the presence of SiO_2 (reaction 2)[24, 25]. Similarly, the more stable AlF_3 (solid and gaseous) forms in the presence of Al_2O_3 [26]. Silicate minerals contain other cations such as Mg, Fe, as well as Si and Al in their crystal structures, and it is thought that fluoride gases containing these cations will form when they are decomposed in TC/EA.

The gases produced in the reactor were transferred to a gas trap. The gas trap is 30 cm long which is filled with 20 cm of ascarite II® adsorbent and 10 cm of $Mg(ClO_4)_2$ granular (Fig. 1(c)). $Mg(ClO_4)_2$ was employed as the moisture adsorbent, and Ascarite II was utilized to remove fluoride gasses in order to safeguard the GC column. Unlike a prior publication, which included a liquid N_2-trap between the reactor and the GC column to remove possible fluoride gas remains [27], we did not use one. We checked the background mass spectrum (scanned around m/z = 12 – 80) before and after the

measurement of fluorine-bearing samples. Although the possible presence of any molecules with a large molecular weight (e.g., SiF_4 or CF_4) could not be examined, at least, the peak derived from C-F-O (fluoromethanone, m/z = 47) which prevents full recovery of oxygen was not identified. After passing through the gas trap, the CO gas flowed into a GC column set at 90˚C and then to an IRMS via an open-slit interface (Con Flo IV, Thermo Fischer Scientific) (Fig. 1(d)). The IRMS model used here was the Delta V Advantage (Thermo Fischer Scientific). This provided the CO peak areas for m/z 28, 29, and 30 (Fig. 1(e), (f)).

2.2.3. Sample encapsulation procedure

Except for IAEA-601 and -602, all samples and silver capsules were heated at 220˚C in an oven for more than 4 h before being encapsulated into the silver capsule to remove adsorbed water molecules. Additives such as fluorine compounds and graphite or additives homogenized with the samples in advance were dried under the same conditions. Immediately after retrieval from the oven, each sample was weighed to obtain an oxygen mass of 100 μg. The measured weight was ranged to within ±5% of the intended weight (100 μg of oxygen) in order to ensure quick weighing. The samples and additives were sealed by folding the silver capsule while pushing out air, and the capsules were again kept dry at 220°C for at least 4 h before being placed in an autosampler. Considering the melting point of benzoic acid (122°C), IAEA-601 and -602 were not heated prior to, during, or following the weighing and sealing procedures. Upon completion of the TC/EA-IRMS, the silver capsules were promptly transferred to an autosampler. Prior to initiating the measurement, the autosampler underwent an overnight purge using He gas to eliminate any remaining gas.

2.2.4 experimental runs

Several recipes for the sample – additive mixture and mixing procedures were compared to identify the most promising method. This can be divided into four series of measurements (Table S2).

Run1: Analysis for comparing the reactivities of the sample-PTFE mixtures with different mixing procedures and different C sources, graphite, or Ni/C. Three different procedures were tested. (1) Sample–PTFE–graphite enclosed in a silver capsule without homogenization. (2) Sample–PTFE–Ni/C was enclosed in a silver capsule without homogenization. (3) Sample–PTFE–Ni/C mixture was homogenized using an agate mortar and pestle before weighing and encapsulation. For these three recipes, the F/O and C/O molar ratios were >2.3 and >1.5, respectively.

Run2: Analysis of reactivities with different F sources. Six inorganic fluorides (LiF, NaF, KF, CaF_2, BaF_2, and AlF_3) and graphite powder were added and homogenized before weighing. The F/O and C/O molar ratios were set to 2 and 1.5, respectively.

Run3: Analysis of reactivities with different F/O molar ratios. NaF was added to the samples at

F/O molar ratios of 2, 3, 4, and 6, and homogenized with graphite or Ni/C before encapsulation.

Run4: Analysis for confirming O yields and $\delta^{18}O$ values using recipes that showed high reactivity in Run1–3. NBS28, SWy-1, and other montmorillonite samples (TKN-01, 29, 31) were analyzed using (1) NaF and graphite with F/O and C/O molar ratios of 6 and 1.5, respectively, and (2) NaF and Ni/C with F/O and C/O molar ratios of 2 and 1.5, respectively.

Besides measurement with samples, the total procedural blank measurement without all components (a silver capsule, a sample, a fluoride compound, and graphite or Ni/C powder) was performed by analyzing the integrated peak area of *m/z* 28. Measurement conditions were the same as those for the non-silicate standards. This indicates that the peak height of contaminated oxygen was less than 1 mV, which did not allow for detection. Thus, the oxygen contamination from the vacuum line is negligible. The oxygen fraction from the sealed silver capsule without any samples and additives was expected to be about 0.26% relative to the IAEA-601. If we assume the $\delta^{18}O$ value of air (23.88%), the blank correction could reduce the analyzed $\delta^{18}O$ value of IAEA-601 by between 0.008 to 0.023‰. Among the additives, the oxygen contamination from Ni/C powder is notable. The oxygen fraction from the Ni/C without any samples was expected to be about 23.79% relative to the IAEA-601 and the Ni/C showed 5.76‰ of $\delta^{18}O$ value. All oxygen yields and $\delta^{18}O$ values in the measurement using Ni/C powder were corrected based on the mass valance between samples and Ni/C.

3. Results and Discussion

3.1. The influence of mixing procedure (Run1)

For each of NBS28 and SWy-1, three conditions were compared (Fig. 2): the samples enveloped with PTFE in silver capsules (Fig. 2(a), (b)) show a CO peak with half the peak height of the reference gas peak. The small peaks around 170–180 s between the reference gas and CO peaks are the peaks of atmospheric N_2 remaining in the silver capsule. Comparing the CO gas generation from non-silicates (NBS18, IAEA-601, and -602) and silicates (NBS28 and SWy-1), the latter showed peaks with lower intensity and tailing on the right side, suggesting that thermal decomposition did not occur instantaneously. The tailed peaks took 40–50 min to return to background levels, resulting in a measurement time of approximately 60 min per sample. Next, whether using Ni/C instead of graphite would improve the reactivity was tested (Fig. 2(c), (d)). The shape of the CO peaks became sharper, and the peak height increased distinctly, especially in SWy-1. Furthermore, the homogenization of Ni/C and PTFE with the sample before weighing and encapsulation resulted in sharper and higher peaks (Fig. 2(e), (f)). The peak height was close to that of non-silicate minerals. This is considered to be due to the closer distance between the sample and the F and C sources, in addition to the

homogenization process, which crushed the grains of NBS28 (several hundred micrometers in diameter) into finer grains. However, the tailings of the peaks were still not completely resolved. It took 40–50 min to return to the background level. It is possible that some oxygen was retained in the residue and then gradually released, even though the majority of the samples broke down. The CO peak area, which is directly proportional to the oxygen output, and the isotope ratio could not be calculated since the peaks' long tailings made it impossible to establish their end positions.

3.2. Influence of F source (Run2)

The reactivities of Qz and SWy-1 were compared for the six fluorinated compounds (Fig. 3 and Fig. S1). NaF and KF were relatively superior in terms of reactivity for both Qz and SWy-1, followed by LiF and PTFE (Run1), while CaF_2, BaF_2, and AlF_3 tended to show significantly lower reactivity. For SWy-1, KF tended to form a shoulder on the right side of the CO peak, whereas NaF tended to decrease the CO peak more smoothly toward the background. Using NaF, the oxygen yields were 54–64% for Qz and 82-91% for SWy-1, showing improvement in reactivity compared to measurements with PTFE. However, a longer time was required for the CO peak to return to background levels compared with the non-silicate standards. For both Qz and SWy-1, the oxygen yields tended to converge to nearly 100% by manually extending the integration width of the CO peak (approximately 900–1000 s from the peak start. Please see Fig. S2 for details). After this convergence, $\delta^{18}O$ varied from 16 to 22‰ for SWy-1 (n = 5), while the reported value is 18.6‰ [11]. The main reason for the large variation in yields and isotope ratio values may be the poor reproducibility of the end positions owing to the long tailing of the peak (Fig. S3).

In addition, the workability of fluorides during weighing and encapsulation was examined. KF showed a significant weight gain during weighing due to its high hygroscopicity (6.9 wt% within 5 min and 13.2 wt% within 10 min after retrieving from the drying oven). For other fluorides, no discernible weight changes were observed within 60 min. Therefore, NaF is the most suitable fluorine source in terms of both reactivity and workability.

3.3. Influence of F/O molar ratio (Run3)

Based on the results of Run2, the reactivity was investigated by varying the F/O ratio using NaF as the fluorine source (Fig. 4). For both Qz and SWy-1, increasing the F/O ratio from 2 to 6 gradually made the CO peak shape more symmetrical, eliminating the tailing and plateau on the right side and bringing the end positions earlier. This led to an improved reproducibility of the end positions and areas of the CO peaks. In contrast to SWy-1, Qz's peak tended to end a little bit later. The difference in reactivity between SWy-1 and Qz may have been influenced by the former's smaller grain size and the larger specific surface area. It is expected that the measurement time per sample can be decreased to approximately 20–30 min, owing to the shortened CO peaks.

The reactivity was improved by increasing the F/O ratio, suggesting that the fluorination of the silicate minerals in the reactor was not stoichiometric. If the reactivity is further improved, fluorination can be achieved, even with an F/O ratio of 2. Therefore, since it was found that replacing graphite with Ni/C could improve the reactivity (Run1), we tested whether the reactivity could be increased by adopting a recipe with Ni/C and NaF at a lower F/O ratio (Fig. S4). The peak end positions for the samples with NaF at F/O = 2 and 6 were not significantly different from those of the samples with NaF at F/O = 6 and graphite, suggesting that Ni/C could cause an efficient and fast reaction, even at low F/O ratios.

3.4. Oxygen yields and $\delta^{18}O$ values using a promising recipe (Run4)

The study from Run1 to Run3 revealed two promising recipes: (1) a recipe using graphite and NaF with F/O = 6 (hereafter, this recipe will be referred to as "FO6"), and (2) one using Ni/C and NaF with F/O = 2 (hereafter, "NiC_FO2"). Using these two recipes, a series of measurements were performed for NBS28, SWy-1, TKN-01, -29, and -31 samples (Run4, 74 samples in total, including 36 standards). The oxygen yields and $\delta^{18}O$ monitored in this series of measurements are shown in Fig. 5. The oxygen yields shown here were calculated based on the CO peak area normalized to the oxygen mass and assuming that the average oxygen yields of IAEA-601 and -602 were 92.8% [14].

First, the oxygen yields of NBS18 calcite were about 60%, indicating that about 2/3 of the oxygen was converted to CO gas by the reaction $CaCO_3 + C_{excess} \rightarrow CaO + 2CO\uparrow$, and the remaining 1/3 became residue as CaO (melting point 2,572°C). For the NaF-bearing samples, the oxygen yields of the first samples in a sequence of five or six consecutive measurements tended to be anomalously high. Especially in the first sequence (NBS28_FO6, run order #16–20), the first sample showed 177% of yield and then gradually declined to approximately 92.8%. In the subsequent sequences, only the first sample showed a significantly higher yield, whereas the yields of the second and subsequent samples tended to stabilize at approximately 90–100% for the sample using FO6 and approximately 85 – 95% for the samples using NiC_FO2. The chromatographs of the NBS28_FO6 and NBS28_NiC_FO2 sequences are shown in Fig. S5. The wider peaks for the earlier samples in the same sequence (Fig. S5). Except for the first sequence of fluorine-bearing samples (NBS28_FO6, run order #16–20), tailings were rarely observed in the second or subsequent samples in each sequence. Although the peak heights were almost the same among replicates, this longer tailing in the first replicate resulted in a higher oxygen yield. It was also likely that the CO peak was terminated in the middle of the tailing, resulting in the underestimation of the $\delta^{18}O$ value in the first replicate. Unlike other sequences, NBS28_FO6 shows the larger maximum of the CO peak in the first replicate, suggesting an oxygen contamination from another source besides the sample. The negative correlation between the oxygen yields and $\delta^{18}O$ values also suggests the oxygen fraction with lower $\delta^{18}O$ value beside the sample (Fig. S6).

It was ruled out that abnormal yields could have been caused by the order in which the weigh-ins were done after the drying oven was removed. This is because, regardless of the weighing procedure's order, the latter portion of the measurement series, which contained the FO6 and NiC_FO2 recipes in the same sequence (run order #48–53, #57–62, #66–71) likewise demonstrated the same trend. Possible factor of the larger oxygen yield and the lower $\delta^{18}O$ values in the first replicate in each sequence is the re-decomposition of the residue of standard samples. NBS18 is expected to leave approximately 40% of the oxygen in the reactor. IAEA-601 and 602 were reported to have an approximate 93% of oxygen yield in thermal decomposition[16,14] , and 7% may remain in the residue. Although we examined the possibility that the standards' residue was decomposed by the NaF input in the following sequence, quantitative consistency could not be found. For example, for the first replicate of NBS28_FO6, if 84% of its 177% oxygen yield came from NBS18 ($\delta^{18}O$ = 7.20‰) and the remaining 93% came from NBS28 (9.57‰), its $\delta^{18}O$ value should be about 8.45‰. Taking account into the IAEA-601 and 602 residues, the $\delta^{18}O$ should be higher than 8.45‰. However, the measured $\delta^{18}O$ value for the first replicate of NBS28_FO6 was 7.54‰, so they did not match. Similar calculations were also performed for other samples with higher oxygen yields, but there was no clear relationship. Although the factors responsible for the increase in oxygen yield are still unclear, the oxygen yield and $\delta^{18}O$ values for each recipe were stable by eliminating the first or second replicate of each sequence.

The oxygen yields and $\delta^{18}O$ values obtained from samples with different recipes are summarized in Table 1. Note that the samples showing the anomalous yields described above (sample run order #16–18, #24, #32, #40, #48, #57, and #66 in Fig. 5a) were removed from this summary. Based on the observed $\delta^{18}O$ of standards (NBS18, IAEA-601, and -602) and their reference values, a calibration curve was determined as follows: $\delta^{18}O_{\mathrm{reference}} = 1.00276 \times \delta^{18}O_{\mathrm{observed}} + 0.18559, R^2 = 1.00000$ (Fig. S7). Then, $\delta^{18}O$ of the silicates were calibrated. Table 1 also shows 1σ of standard deviation of yields and $\delta^{18}O$ values.

For the samples used the FO6 recipe, the oxygen yields of NBS28 were 98.2 – 99.3% and that of SWy-1 were 90.0 – 91.6%. NBS28 showed higher oxygen yields, which may be due to the longer CO peak with slight tailing rather than a higher reactivity than that of SWy-1. For the samples used the NiC_FO2 recipe, the oxygen yields of both NBS28 and SWy-1 are approximately 90%.

The samples with NaF at F/O = 2 in Run2 (Fig.3) showed a large deviation of $\delta^{18}O$ values (16 – 22 ‰), while the FO6 and the NiC_FO2 recipes in Run4 resulted in the smaller deviation (0.30 and 0.33 ‰, respectively). SWy-1 tended to have a higher precision than NBS28 in both recipes. This is probably due to the smaller particle size of SWy-1 (< 2 μm) than NBS28. In addition, the NBS28_FO6 samples were analyzed in the first sequence among the other NaF-bearing samples in the series of measurement runs (Fig. 5), which could be related to the lower precision. By using a continuous-flow TC/EA-IRMS method and KF as the fluorine source, 0.33 ‰ of 1σ for NBS28 and 0.29 ‰ for NBS27

biotite were reported [12]. The precision in this study was comparable to the above report, while the precisions of the conventional methods (dual-inlet system, BrF_5 and CO_2 laser fluorination) were at most 0.2‰ [28].

It is known that $\delta^{18}O$ values in quartz show a large discrepancy among laboratories, depending on the fluorination methods; The $\delta^{18}O$ values for NBS28 varied from 8.8 to 10.0‰ [28, 29]. If we regarded it as 9.57‰ according to the reference sheet from IAEA [30], this study showed a discrepancy of +1.4‰ for the FO6 recipe and +1.0‰ for the NiC_FO2 recipe. For the case of the negative shift of $\delta^{18}O$ values from the reference value, it could be explained as a lighter isotope was selectively obtained due to insufficient decomposition reactions because Si-^{16}O bonds are more easily broken than Si-^{18}O bonds. On the other hand, the positive shift observed in this study is not likely due to isotope fractionation in the insufficient decomposition. The similar TC/EA-IRMS method reported 10.23‰ for NBS28 [12], showing a positive shift of $\delta^{18}O$ value. Another literature reported that the mean value of $\delta^{18}O$ in NBS28 was almost equal to the reference value [13]. They also used TC/EA-IRMS but measured the CO gas once it was stored in a trap. Although we do not know the exact reason, the positive shift of $\delta^{18}O$ in NBS28 may be due to the specific characteristics of the continuous flow system.

For SWy-1, the reported values were very limited compared with those of NBS28. A laser fluorination method provided 18.6 ± 0.23‰ [11], while a conventional BrF_5 fluorination method showed 19.2‰ [31]. Compared to these, the present study obtained lighter values; 17.8‰ for the FO6 recipe and 18.0‰ for the NiC_FO2 recipe. One possibility for the displacement of $\delta^{18}O$ observed in SWy-1 is the effect of adsorbed water, which is a unique problem for smectite. A previous report demonstrated that exposure to atmospheric air for about 25 minutes after drying resulted in smectite rehydration with less than 1 wt% of adsorbed water [32]. If we assume that adsorbed water has $\delta^{18}O$ value of approximately -10 to -15‰, which is a plausible value for an isotope in precipitation, then 0.5 wt% of the adsorbed water reduces the $\delta^{18}O$ of SWy-1 by about 0.26 – 0.30‰. Obviously, this negative shift of $\delta^{18}O$ depends on the amount of adsorbed water and its isotope composition; however, considering the effect of adsorbed water and the precision among replicates (1SD, ±0.18‰), the $\delta^{18}O$ value of SWy-1_FO6 obtained in this study was in the range of 2SD.

3.5 Potentials and further improvements in the methodology

Although this study used at least 100 mg of each sample and additive in the process of homogenization in an agate mortar before encapsulation, one measurement is possible with about 200 μg of sample in a silver capsule. It is important to design pretreatment procedures for homogenizing tiny volumes of material. The measurement time was approximately 20–30 min for one silicate sample and 10 min for one non-silicate standard. Therefore, it has the potential to measure, at maximum, 15 unknown samples within 24 h. This is a major advantage of our proposed method. The conventional BrF_5 fluorination method requires several milligrams of the sample and approximately 12 h for fluorination. The CO_2

laser fluorination method requires a small amount of sample. Each measurement is estimated to consume about 0.2 mg of sample or more and takes about 45 – 90 min, depending on the cycles of dual inlet measurement [33, 34]. The cycling between samples and reference gas measurement provides a high precision 0.01 - 0.1‰ of 2σ. Compared to these established methods, the oxygen isotope measurement method using TC/EA may be useful in cases where a large number of samples have to be processed with a moderate degree of precision.

We also confirmed that hydrogen isotope ratios could be measured using the same instrument and configuration (data not shown). Hydrogen measurement needs fluorine-free samples to prevent HF formation, which hampers full hydrogen recovery. Also, approximately 20 μg of hydrogen mass was needed, and in the case of smectite or mica, it is equivalent to approximately 4–5 mg of the sample, while only 0.2 mg is required for oxygen measurement. Therefore, the simultaneous measurement of hydrogen and oxygen isotope ratios for one capsule is difficult; however, by preparing fluorine-free and fluorine-bearing samples for hydrogen and oxygen analyses, respectively, it is possible to measure both in a series of runs.

Despite the improvement in the oxygen yields from silicates in this study, problems persist. First, at the beginning of the series of samples containing fluorine, excessive amounts of oxygen yield occurred. This suggests extra sources of oxygen (e.g., residues of standard samples), but they were not elucidated in this study. At least, the residues of standard samples alone could not explain their mass balance. Currently, a stable analysis can only be performed by checking the pyrolysis chromatograph and arbitrarily rejecting samples with abnormal behavior. Therefore, it is necessary to optimize the loading method and selection of additives and standard samples without oxygen contamination, to prevent the waste of samples. Next, the accuracy of the $\delta^{18}O$ value needs to be examined with a wider variety of silicate minerals. However, there are few international standards for silicate minerals, which may hinder this verification. Inter-laboratory comparisons using multiple methods for silicate minerals other than NBS28, which are the most frequently reported, are needed. Because the main focus of this study was to find a promising recipe for separating oxygen from silicates, normalization based on international water standards such as VSMOW2 and SLAP2 were not achieved. To eliminate instrumental bias, VSMOW-SLAP scaling should be addressed in future studies. Third, optimization of a recipe with as little fluoride additive as possible may be required. In this study, the higher the F/O ratio, the better the reactivity with silicate. Although the IRMS detector did not show any fluoride contamination, the negative effects of the fluoride gas produced on the instrument cannot be completely ruled out. Regardless of whether it is in a continuous-flow system or a dual-inlet system, the optimization of the recipe will be performed in the future. The recipe produced in this study is anticipated to exhibit a comparable outcome for TC/EA-IRMS in the dual-inlet system.

Conclusions

In this study, the oxygen yield of silicate was improved using the same TC/EA-IRMS instrument that is widely used for organic matter. Improvements in CO gas generation from silicate minerals can be achieved by (1) using NaF as a fluorine source, (2) using Ni/C, which has a catalytic effect, as a carbon source, and by homogenizing the additive and sample before encapsulation, and (3) increasing the F/O ratio. It was found that a recipe using NaF with an F/O ratio of 6 provided sufficient reactivity and oxygen yield and reduced the measurement time from 60 min to 20–30 min per sample. However, a drawback was also identified in the early cycles of loading the sample bearing NaF. The initial replicates of NaF-bearing silicate samples showed anomalously higher oxygen yields and lower $\delta^{18}O$ values, requiring more improvement in the methodology. Because the TC/EA-IRMS method is highly automated and does not require a specialist apparatus, further refining of this methodology will increase access to isotope measurements. This will further promote isotope studies of oxygen-bearing Earth materials and accelerate the exploration of the biological and geochemical processes between them.

Author contributions

Ryosuke Kikuchi: Conceptualization, methodology, resources, formal analysis, investigation, data curation, funding acquisition, and writing of the original manuscript.

Tobimaru Ishiwata: formal analysis, investigation, writing—review and editing.

Ichiro Tayasu: methodology, resources, investigation, writing—review and editing.

Acknowledgements

We gratefully acknowledge the Research Institute for Humanity and Nature staff for the use of the TC/EA-IRMS. This study was conducted by the support of Joint Research Grant for the Environmental Isotope Study of Research Institute for Humanity and Nature. We thank Prof. Tsubasa Otake for financial and administrative support. This work was supported by JSPS KAKENHI Grant Numbers JP20H00184. We thank Dr. Masakazu Ito for providing the bentonite ore.

Reference

1. Coplen TB. Guidelines and recommended terms for expression of stable-isotope-ratio and gas-ratio measurement results. *Rapid Commun Mass Spectrom*. 2011;25(17):2538-2560. doi:10.1002/rcm.5129
2. Criss RE. Terrestrial Oxygen Isotope Variations and Their Implications for Planetary Lithospheres. In: J. MG, Mittlefehldt DW, Jones JH, Simon SB, Papike JJ, Mackwell S, eds. *Reviews in Mineralogy and Geochemistry Oxygen in the Solar System*. Vol 68. Mineralogical Society of America; 2008:511-526. doi:10.2138/rmg.2008.68.18

3. Eiler JM. Oxygen Isotope Variations of Basaltic Lavas and Upper Mantle Rocks. In: Valley JW, Cole DR, eds. *Stable Isotope Geochemistry*. Vol 43. Mineralogical Society of America; 2001:319-364. doi:10.1515/9781501508745-008
4. Troll VR, Weis FA, Jonsson E, et al. Global Fe–O isotope correlation reveals magmatic origin of Kiruna-type apatite-iron-oxide ores.pdf. *Nat Commun*. 2019;10(1712).
5. Jaffrés JBD, Shields GA, Wallmann K. The oxygen isotope evolution of seawater: A critical review of a long-standing controversy and an improved geological water cycle model for the past 3.4 billion years. *Earth-Science Rev*. 2007;83(1-2):83-122. doi:10.1016/j.earscirev.2007.04.002
6. Ryb U, Eiler JM. Oxygen isotope composition of the Phanerozoic ocean and a possible solution to the dolomite problem. *Proc Natl Acad Sci U S A*. 2018;115(26):6602-6607. doi:10.1073/pnas.1719681115
7. Ronov & Yaroshevsky 1969 Chemical composition of the Earth's crust.
8. Clayton RN, Mayeda TK. The use of bromine pentafluoride in the extraction of oxygen from oxides and silicates for isotopic analysis. *Geochim Cosmochim Acta*. 1963;27(1):43-52. doi:10.1016/0016-7037(63)90071-1
9. Sharp ZD. A laser-based microanalytical method for the in situ determination of oxygen isotope ratios of silicates and oxides. *Geochim Cosmochim Acta*. 1990;54(5):1353-1357. doi:10.1016/0016-7037(90)90160-M
10. Kirschner DL, Sharp ZD. Oxygen isotope analyses of fine-grained minerals and rocks using the laser-extraction technique. *Chem Geol*. 1997;137(1-2):109-115. doi:10.1016/S0009-2541(96)00123-4
11. Bauer KK, Vennemann TW, Gilg HA. Stable isotope composition of bentonites from the Swiss and Bavarian Freshwater Molasse as a proxy for paleoprecipitation. *Palaeogeogr Palaeoclimatol Palaeoecol*. 2016;455:53-64. doi:10.1016/j.palaeo.2016.02.002
12. Gehre M, Strauch G. High-temperature elemental analysis and pyrolysis techniques for stable isotope analysis. *Rapid Commun Mass Spectrom*. 2003;17(13):1497-1503. doi:10.1002/rcm.1076
13. Menicucci AJ, Matthews JA, Spero HJ. Oxygen isotope analyses of biogenic opal and quartz using a novel microfluorination technique. *Rapid Commun Mass Spectrom*. 2013;27(16):1873-1881. doi:10.1002/rcm.6642
14. Yin X, Chen Z. Measuring oxygen yields of a thermal conversion/elemental analyzer-isotope ratio mass spectrometer for organic and inorganic materials through injection of CO. *J Mass Spectrom*. 2014;49(12):1298-1305. doi:10.1002/jms.3463
15. Kornexl BE, Gehre M, Höfling R, Werner RA. On-line δ18O measurement of organic and inorganic substances. *Rapid Commun Mass Spectrom*. 1999;13(16):1685-1693. doi:10.1002/(sici)1097-0231(19990830)13:16<1685::aid-rcm699>3.0.co;2-9
16. Ellis NM, Passey BH. A novel method for high-precision triple oxygen isotope analysis of diverse

Earth materials using high temperature conversion–methanation–fluorination and isotope ratio mass spectrometry. *Chem Geol*. 2023;635:121616. doi:10.1016/j.chemgeo.2023.121616

17. Brand WA, Coplen TB, Aerts-Bijma AT, et al. Comprehensive inter-laboratory calibration of reference materials for d 18O versus VSMOW using various on-line high-temperature conversion techniques. *Rapid Commun Mass Spectrom*. 2009;23(7):999-1019. doi:10.1002/rcm

18. Brand WA, Coplen TB, Vogl J, Rosner M, Prohaska T. Assessment of international reference materials for isotope-ratio analysis (IUPAC technical report). *Pure Appl Chem*. 2014;86(3):425-467. doi:10.1515/pac-2013-1023

19. Gonfiantini R, Stichler W, Rozanski K. Standards and intercomparison materials distributed by the International Atomic Energy Agency for stable isotope measurements. In: *Reference and Intercomparison Materials for Stable Isotopes of Light Elements*. Vienna: IAEA; 1995:13-29. doi:10.1016/0375-6505(95)00024-0

20. Takagi T. *Bentonite in Japan –Geology and Industries–*. Geological Survey of Japan; 2005. https://www.gsj.jp/researches/openfile/openfile2005/openfile0425.html.

21. Richardson Y, Motuzas J, Julbe A, Volle G, Blin J. Catalytic investigation of in situ generated Ni metal nanoparticles for tar conversion during biomass pyrolysis. *J Phys Chem C*. 2013;117(45):23812-23831. doi:10.1021/jp408191p

22. Cases JM, Bérend I, Francois M, Uriot JP, Michot LJ, Thomas F. Mechanism of Adsorption and Desorption of Water Vapor by Homoionic Montmorillonite: 3. The Mg2+, Ca2+, Sr2+ and Ba2+ exchanged forms. *Clays Clay Miner*. 1997;45(1):8-22. doi:10.1021/la00047a025

23. Kanik NJ, Longstaffe FJ, Kuligiewicz A, Derkowski A. Systematics of smectite hydrogen-isotope composition: Structural hydrogen versus adsorbed water. *Appl Clay Sci*. 2022;216:106338. doi:10.1016/j.clay.2021.106338

24. Hirai D, Sawai O, Nunoura T, Hiroi Z. Facile synthetic route to transition metal oxyfluorides via reactions between metal oxides and PTFE. *J Fluor Chem*. 2018;209:43-48. doi:10.1016/j.jfluchem.2018.02.008

25. Mogab CJ, Adams AC, Flamm DL. Plasma etching of Si and SiO2 - The effect of oxygen additions to CF4 plasmas. *J Appl Phys*. 1978;49(7):3796-3803. doi:10.1063/1.325382

26. Hobosyan MA, Kirakosyan KG, Kharatyan SL, Martirosyan KS. PTFE-Al2O3 reactive interaction at high heating rates. *J Therm Anal Calorim*. 2015;119:245-251.

27. Werner RA. The online 18O/16O analysis: Development and application. *Isotopes Environ Health Stud*. 2003;39(2):85-104. doi:10.1080/1025601031000108642

28. Kusakabe M, Matsuhisa Y. Oxygen three-isotope ratios of silicate reference materials determined by direct comparison with VSMOW-oxygen. *Geochem J*. 2008;42(4):309-317. doi:10.2343/geochemj.42.309

29. Tanaka R, Nakamura E. Determination of 17O-excess of terrestrial silicate/oxide minerals with

respect to Vienna Standard Mean Ocean Water (VSMOW). *Rapid Commun Mass Spectrom*. 2013;27(2):285-297. doi:10.1002/rcm.6453

30. IAEA. *Reference Sheet for Reference Materials: NBS28 & NBS30*. Vienna; 2007. internal-pdf://nbs28_nbs30-3415789127/NBS28_NBS30.pdf.

31. Whitney G, Northrop HR. Experimental investigation of the smectite to illite reaction: Dual reaction mechanisms and oxygen-isotope systematics. *Am Mineral*. 1988;73:77-90.

32. Bauer KK, Vennemann TW. Analytical methods for the measurement of hydrogen isotope composition and water content in clay minerals by TC/EA. *Chem Geol*. 2014;363:229-240. doi:10.1016/j.chemgeo.2013.10.039

33. Tanaka R, Nakamura E. Silicate-SiO reaction in a protoplanetary disk recorded by oxygen isotopes in chondrules. *Nat Astron*. 2017;1(May). doi:10.1038/s41550-017-0137

34. Greenwood RC, Franchi IA, Findlay R, et al. Oxygen isotope evidence from Ryugu samples for early water delivery to Earth by CI chondrites. *Nat Astron*. 2023;7(1):29-38. doi:10.1038/s41550-022-01824-7

Tables, and Figure captions

Table 1. Oxygen yields and $\delta^{18}O$ of silicate samples at different method

Fig. 1 The schematics of TC/EA-IRMS configuration.
(A) Autosampler, (B) TC/EA reactor, (C) Gas trap and GC column, (D) Con Flo IV, (E) IRMS, (F) pyrolysis chromatograph

Fig. 2. The *m*/*z* 28, 29 and 30 traces during analysis of NBS28 (left column) and SWy-1 (right column). (A, B) The samples enveloped with PTFE in silver capsule. (C, D) Use of Ni/C instead of graphite, (E, F) Use of Ni/C and the homogenization before encapsulation. The intensity of reference gas of *m*/*z* 29 was set approximately 6000 mV for each measurement.

Fig. 3. The *m*/*z* 28, 29 and 30 traces during analysis of Qz with different inorganic fluoride. (A) LiF, (B) NaF, (C) KF, (D) BaF_2, (E) CaF_2, (F) AlF_3. The intensity of reference gas of *m*/*z* 29 was set approximately 6000 mV for each measurement.

Fig. 4. The *m*/*z* 28 traces during analysis of (A) Qz and (B) SWy-1 with different F/O ratio. Red arrows represent the positions of CO peak ends.

Fig. 5. Oxygen yields (A) and observed $\delta^{18}O$ (B) in a series of measurement run. Open, red, and gray rectangles denote NBS18, IAEA-601, and 602, respectively. Solid and open triangles denote quartz (NBS28) and montmorillonite (SWy-1, TKN-01, -29, -31), respectively. The dashed line represents the 92.8% yield as the average value for benzoic acids (IAEA-601 and -602).

Table 1. Oxygen yields and $\delta^{18}O_{VSMOW}$ of silicate samples at different method

F/O	F source	C source	O yield [%]*		$\delta^{18}O$ [‰]	
			NBS28	SWy-1	NBS28 9.57 ‰†	SWy-1 18.6 ‰‡
2	NaF	Graphite	54 – 64	82 – 91	N.D.	16 – 22
6	NaF	Graphite	98.2 – 99.3	90.0 – 91.6	11.0 ±0.30	17.9 ±0.18
2	NaF	Ni/C	86.4 – 90.2	86.7 – 88.9	10.6 ±0.33	18.0 ±0.10

*O yield was calculated based on CO peak area normalized by oxygen mass and the assumption of the average oxygen yields of IAEA-601 and 602 are 92.8% (Yin & Chen, 2014).

† IAEA (2007), ‡ Bauer et al. (2016).

Figures

Oxygen isotope analysis for silicate minerals using a high temperature conversion/elemental analyzer-isotope ratio mass spectrometer

Ryosuke Kikuchi*[1], Tobimaru Ishiwata[2], Ichiro Tayasu[3]

[1] Faculty of Engineering, Hokkaido University, Sapporo 060-8628, Hokkaido, Japan, [2] Graduate School of Engineering, Hokkaido University, Sapporo 060-8628, Hokkaido, Japan, [3] Research Institute of Humanity and Nature, Kita-ku, Kyoto, 603-8047 Japan.

*Corresponding author

Tel: +81-11-706-6320 (Ext: 6320)

E-mail address: rkikuchi@eng.hokudai.ac.jp

Fig. 1

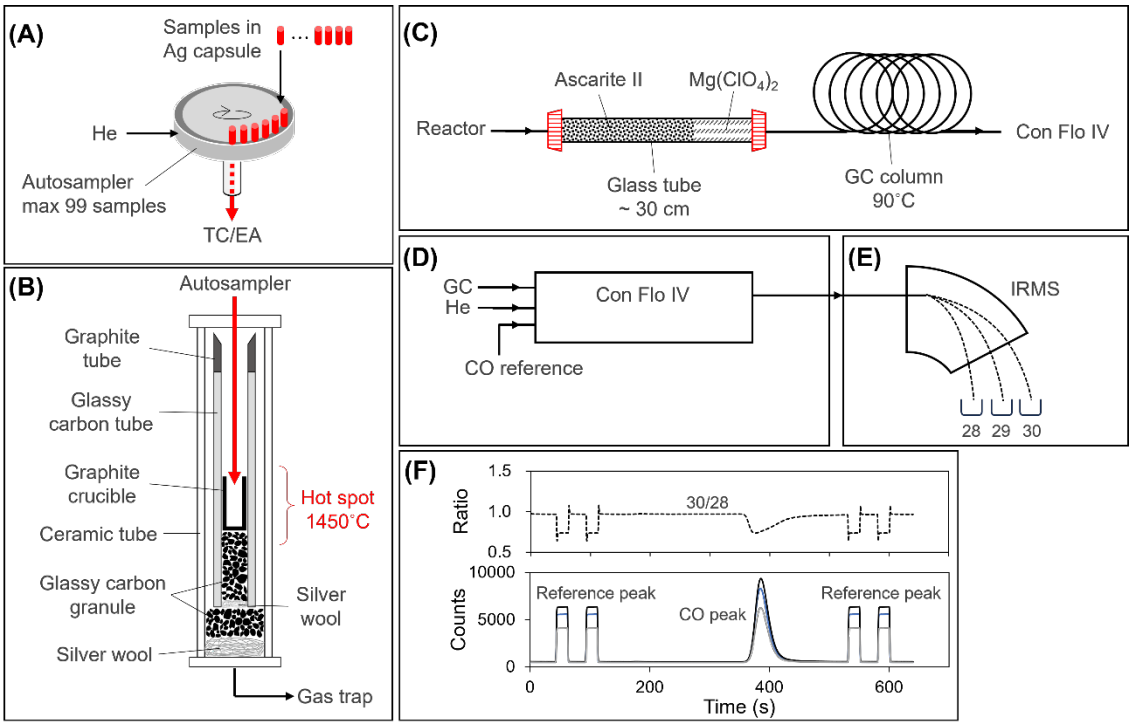

Fig. 2

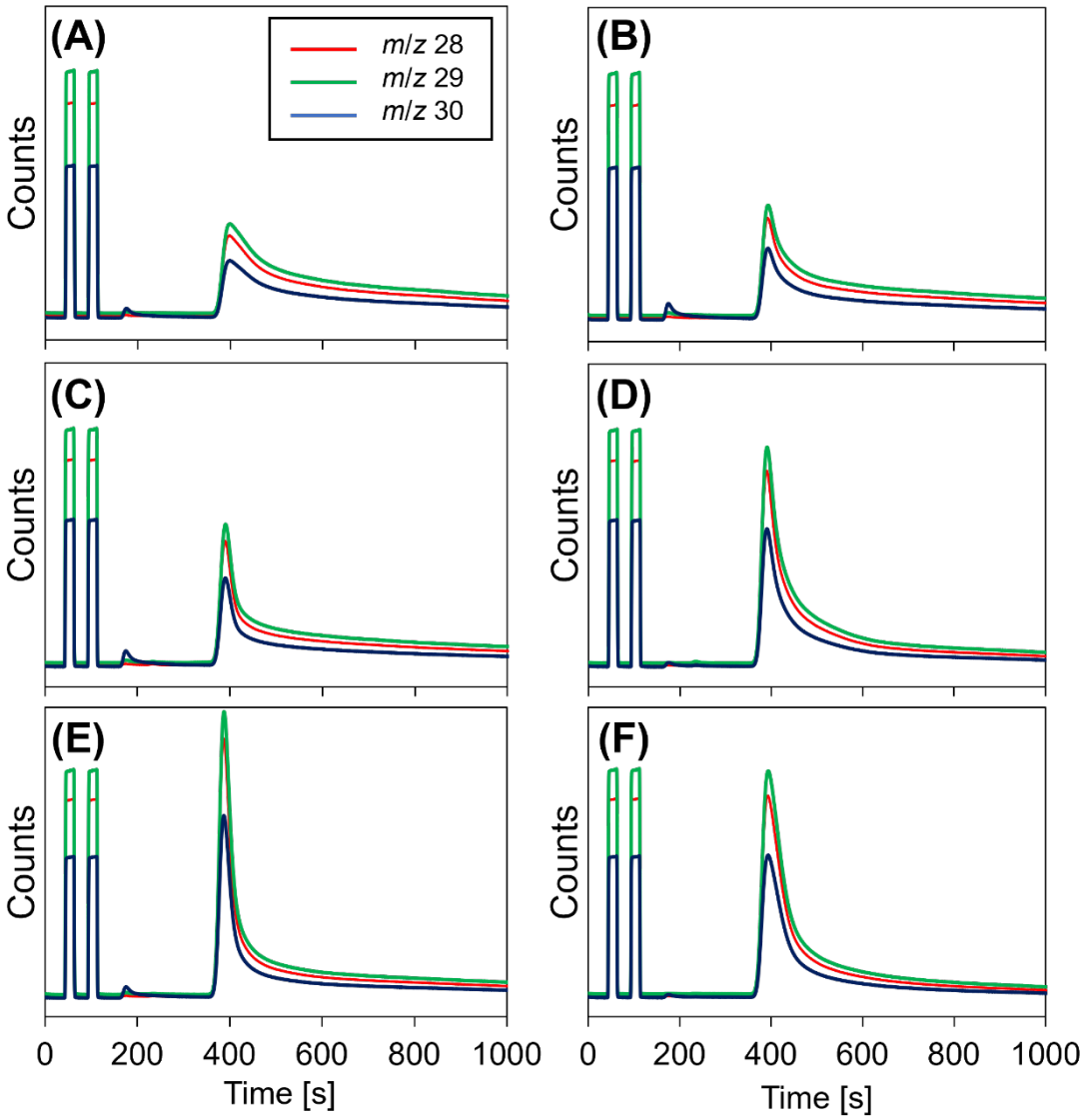

Fig. 3

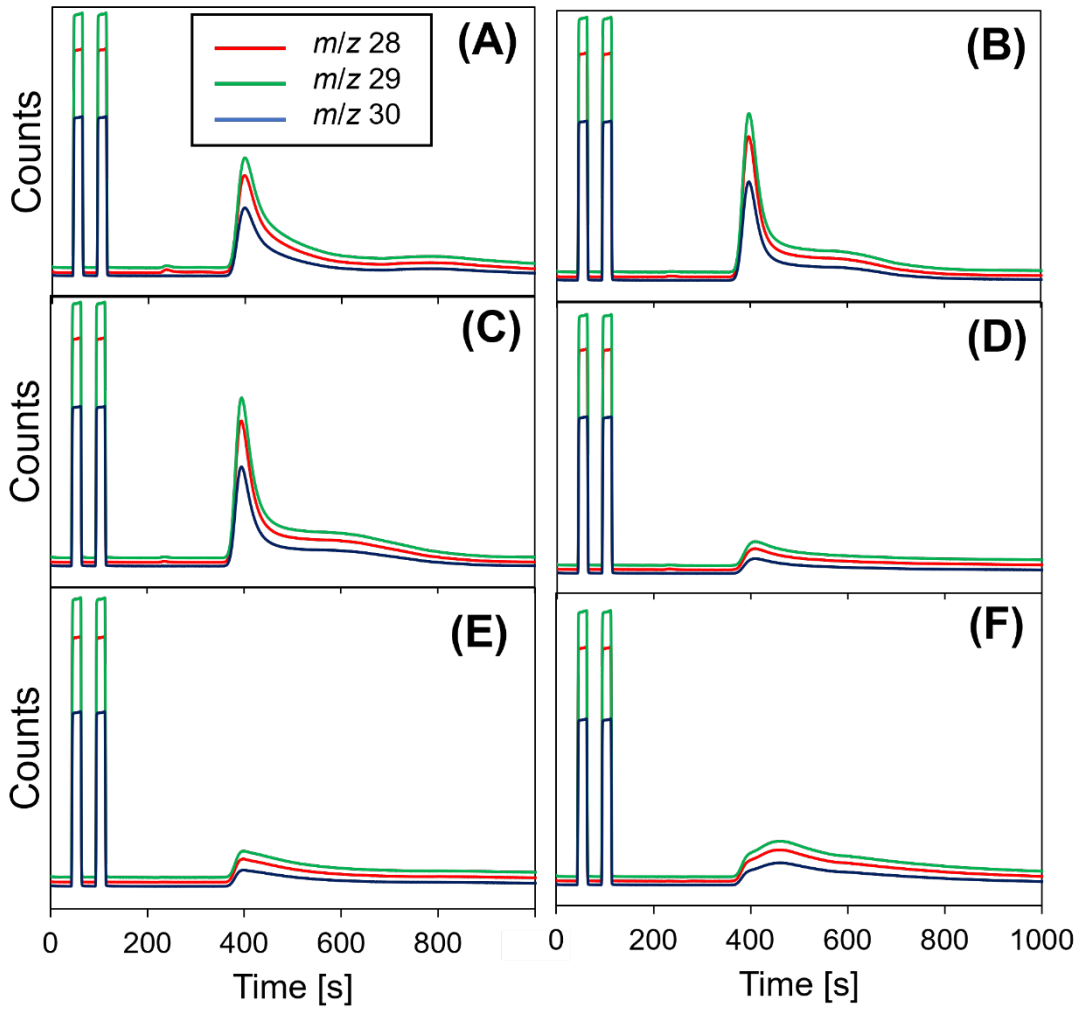
m/z 28
m/z 29
m/z 30
(A)
(B)
(C)
(D)
(E)
(F)
Counts
Counts
Counts
0
200
400
600
800
0
200
400
600
800
1000
Time [s]
Time [s]

Fig. 4

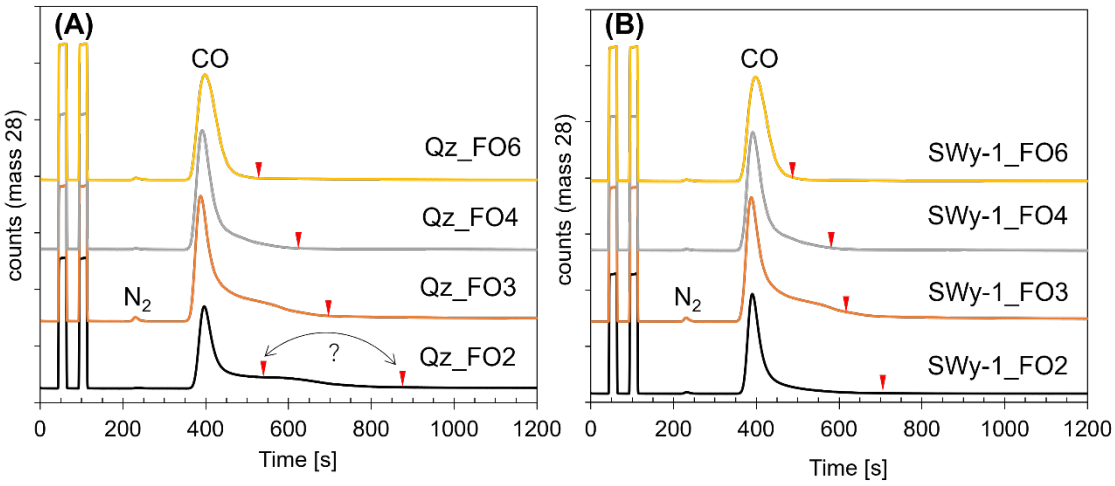
(A)
CO
Qz_FO6
Qz_FO4
Qz_FO3
Qz_FO2
N2
?
counts (mass 28)
0
200
400
600
800
1000
1200
Time [s]
(B)
CO
SWy-1_FO6
SWy-1_FO4
SWy-1_FO3
SWy-1_FO2
N2
counts (mass 28)
0
200
400
600
800
1000
1200
Time [s]

Fig. 5

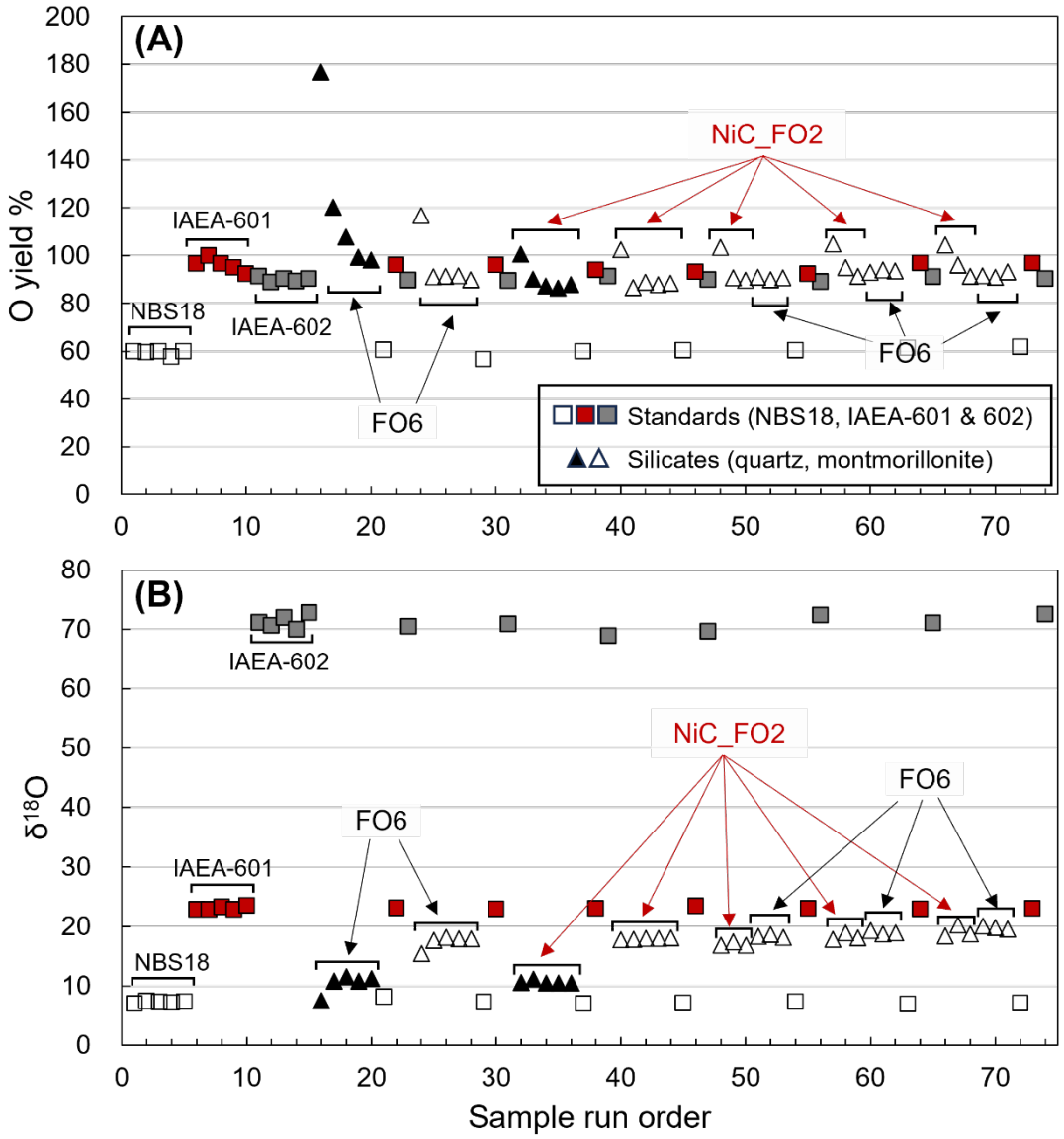
(A)
O yield %
NiC_FO2
IAEA-601
NBS18
IAEA-602
FO6
FO6
Standards (NBS18, IAEA-601 & 602)
Silicates (quartz, montmorillonite)
(B)
δ18O
IAEA-602
NiC_FO2
FO6
FO6
IAEA-601
NBS18
Sample run order